Available online at www.sciencedirect.com
ScienceDirect
Journal of the European Ceramic Society 30 (2010) 497–502
www.elsevier.com/locate/jeurceramsoc

Pulsed-laser deposited amorphous-like PZT thin-films: Microstructure and optical properties

J. Lappalainen [a,*], J. Puustinen [a], J. Hiltunen [b], V. Lantto [a]

[a] *Microelectronics and Materials Physics Laboratories, EMPART Research Group of Infotech Oulu, University of Oulu, Linnanmaa, FIN-90570, Oulu, Finland*
[b] *VTT Technical Research Centre of Finland, Kaitoväylä 1, FIN-90571, Oulu, Finland*

Available online 23 July 2009

Abstract

Amorphous lead–zirconate–titanate ($Pb_{0.97}Nd_{0.02}(Zr_{0.55}Ti_{0.45})O_3$, PNZT) thin-films were grown on single-crystal MgO(1 0 0) substrates at room temperature by pulsed laser deposition (PLD). Part of PNZT films was left as-deposited amorphous and others were post-annealed at temperatures from 100 to 400 °C. X-ray diffraction (XRD) and scanning probe microscopy (SPM) were used to characterize the microstructure. Optical properties were analyzed using spectrophotometry at UV–vis–NIR and prism-coupler method at 633 nm wavelengths. Initially, films were amorphous with a broad XRD peak around $2\theta \approx 29.7°$. As the post-annealing temperature increased above 250 °C, the amorphous peak started to shift towards lower 2θ-angles and got narrower indicating of decreasing interatomic spacing and possible glass transformation. At the same time, the transmittance at all wavelengths increased remarkably, although no crystal structure was detected by XRD. Also, sharp optical TE_0 modes with full-width half-maximum (FWHM) values of $\Delta\beta \approx 0.00067$ could be coupled into these films.

Keywords: Films; Amorphous; Optical properties; PZT

1. Introduction

Amorphous solid-state materials and glass forming alloys are utilized in several technology areas including magnetic and optical memories, optical components, various steps of fabrication and parts in integrated circuits, and solar cells, for example. Very often amorphous materials are used as passive medium without any controllable functionality, like in optical windows and high refractive index lenses and waveguides, gate dielectrics in MOS component structures and other electrical insulation applications, exploiting materials such as silicon oxide (SiO_2) and silicate- or alumina-based glasses. On the other hand, in various new material groups, like rare-earth transition-metal bulk metallic glasses (BMG), some pseudobinary alloy systems, and shape-memory alloys, for example, the phase transformation between amorphous and crystalline state can be controlled by heat or light to generate memory effect based on change of magnetic or optical properties.[1–4] Conventionally crystalline functional $BaTiO_3$ and $Pb(Zr_xTi_{1-x})O_3$ ceramics have also been successfully prepared in the amorphous form in a way preserving their ferroelectricity.[5]

Throughout the literature it is frequently brought up that the phenomena affecting in the early stages of formation of crystalline structure are not fully understood. Nevertheless, there are distinctive regions observed in the development of materials properties as a function of heat-treatment temperature that are similar to all material groups. When an initially amorphous material is heated above the so-called glass transformation temperature T_g, material transforms to a viscous liquid state. If temperature is increased somewhat further, the nucleation will take place and the crystallization process starts.[6] However, if temperature is instead decreased back below the glass transformation temperature T_g, material will form a glassy state.[7] This means that materials various properties, like optical transmittance, reflectance, surface morphology,[2] electrical conductivity, hardness, etc., can be changed remarkably although there is no crystalline structure developed, and the material can still be defined as an amorphous solid. Glass transformation process can be observed, for example, by differential scanning calorimetry (DSC)[2,3,6] and XRD measurement[8] experiments. In the case of XRD technique, the evolution of the amorphous phase along the glass transformation process can be studied by

* Corresponding author.
E-mail address: jyla@ee.oulu.fi (J. Lappalainen).

0955-2219/$ – see front matter © 2009 Elsevier Ltd. All rights reserved.
doi:10.1016/j.jeurceramsoc.2009.06.029

following the changes in the 2θ-angle position and the full-width half-maximum (FWHM) values of the amorphous peak.

In their early works Lines[9] and Glass et al.[10] have very clearly shown, both theoretically and experimentally, respectively, that ferroelectricity can also be present in glassy and amorphous state of the matter, as well. Only it is important that the entity fundamentally responsible of ferroelectricity in the matter, like distorted BO_6 oxygen octahedra in the case of ferroelectric perovskite ABO_3 compounds, still exists, no matter how distorted, but still in an identifiable form. This assumption was further developed to consider chemical bonds, such as Ba–Ti–O, formed in organic solutions used to fabricate gel-derived glasses in the form of thin films at temperatures as low as 200 °C.[11] The ferroelectric response was found to be due to existence of so-called "ferrons", arranged entities of the size in the scale of around ~50 Å composed of TiO_6 octahedrals, visible also in transmission electron microscopy (TEM) micrographs. Although the existence of ferroelectricity in the films was clearly proved, other properties of the films, including optical transmittance $T(\lambda)$, refractive index n, remanent polarization P_r, dielectric constant ε, and loss angle $\tan\delta$, were found to be controlled mainly by the organic residuals or pores still present in the films. Amorphous ferroelectric films have been produced by some other methods as well, including sputtering.[4,12]

Amorphous alloys and glasses are typically fabricated using melt-quenching technique,[2,3,10] or like often in the case of thin films, mostly by spin coating sol–gel liquids.[5,11] Although XRD analysis of these materials reveals them to be in amorphous state, there are some features in these processes that should be considered from the materials structure point of view. In melt-quenching process, materials are heated up to high temperatures over the melting temperature, and then rapidly cooled down to form an amorphous solid. Density of nucleation centers and nanosized crystals developed in the material are mainly determined by the cooling rate. In the sol–gel process, on the other hand, final amorphous material consists of various residual substances originating from the fabrication process affecting on various properties of amorphous constituent. Using sputtering[4] or, like reported in this paper, pulsed laser deposition (PLD) techniques, it is possible to fabricate essentially amorphous thin films that are grown at temperatures only few tenths above room temperature, and contain only the elements present in the target. Also, the films are typically very dense without voids and pores, and the surface morphology is of optical quality with the surface roughness $R_q < 5$ nm. These properties ensure that solely characteristics of the studied amorphous material are observed.

2. Experimental

PLD process was used to grow Nd-modified lead–zirconate–titanate ($Pb_{0.97}Nd_{0.02}(Zr_{0.55}Ti_{0.45})O_3$, PNZT) thin-films on single-crystal MgO(1 0 0) substrates at room temperature. Commercial PNZT target with high purity and density of 7.5×10^3 kg/m^3 was used for the film fabrication. The deposition was carried out in a vacuum chamber evacuated down to pressure of 6×10^{-5} mbar, and the substrate and the target were placed parallel at a distance of 30 mm. Laser beam fluence of 1.5 J/cm^2 of a XeCl excimer laser (LambdaPhysik COMPex 201) operating at the wavelength of 308 nm was selected for the deposition to maintain the morphotropic phase boundary (MPB) composition of the target in films.[13] The repetition rate of laser pulses was 5 Hz and the duration of the single pulse was around 30 ns. A calibrated quartz crystal microbalance (QCM) resonator based film thickness/rate monitor (Sycon STM-100) was used to control the thickness of the films to 200, 300, and 500 nm. Part of the PNZT films was left as-deposited amorphous and others were post-annealed at temperatures from 100 to 400 °C under the inverted zirconia crucible together with some PNZT powder. The heating and cooling rate of 300 °C/h was used in every temperature profile. Crystal structure of all films was studied by conventional X-ray diffraction (XRD) θ–2θ measurements (Philips PW1380) using scanning speed of 1/8°/min in order to maximize the signal to noise ratio. CuKβ-reflection of MgO(2 0 0) substrate was used for the correction of XRD data. Gaussian amplitude functions were used to fit the XRD intensity data to obtain accurately 2θ-angle and FWHM values. Scanning probe microscopy (SPM) studies (Veeco Dimension 3100) were carried out in order to study the surface morphology evaluation and the surface roughness values R_q of the films as a function of different post-annealing temperatures.

Optical transmission spectrum $T(\lambda)$ of PNZT thin-films at the wavelength range from 170 to 3000 nm was measured perpendicular to the film surface using spectrophotometer (Varian Cary 500). Refractive index n and extinction coefficient k were calculated from $T(\lambda)$ data fitted with multiple Lorentz-oscillator model used in calculation software (SCI Film Spectrum). A prism-coupler method (Metricon 2010) operating at the wavelength of 632.8 nm was utilized in order to study the coupling efficiency of light in the PNZT film in the plane of film surface. Both TE_0 and TM_0 guided modes were excited in the films to reveal possible birefringence effects.

3. Results and discussion

Evaluation of structural changes occurring in as-deposited and post-annealed films as a function of heat-treatment temperature T_{an} were studied using conventional θ–2θ XRD measurements. As it is very well known, even the perfectly disordered matter produces a broad peak with low intensity at the 2θ-angles around 20–30° representing the distribution of interatomic distances fulfilling Bragg condition, and leading to local diffraction intensity maximum. In Fig. 1(a), there are XRD patterns measured from one as-deposited PZT thin-film and five films post-annealed at temperatures of 100, 200, 300, 350, and 400 °C. The 2θ-angle positions of the measured patterns were corrected by using CuKβ-reflection of MgO(2 0 0) substrate at $2\theta \approx 38.551°$. It is clear from the patterns that no crystalline phases of perovskite PZT or pyrochlore are present in the films. Position of amorphous peak is varying to some extent even at low temperatures of RT, 100, and 200 °C, but when the post-annealing temperature is further increased, the peak starts to move towards smaller 2θ-angles, and also gets narrower. This tendency was found systematically in all samples with different

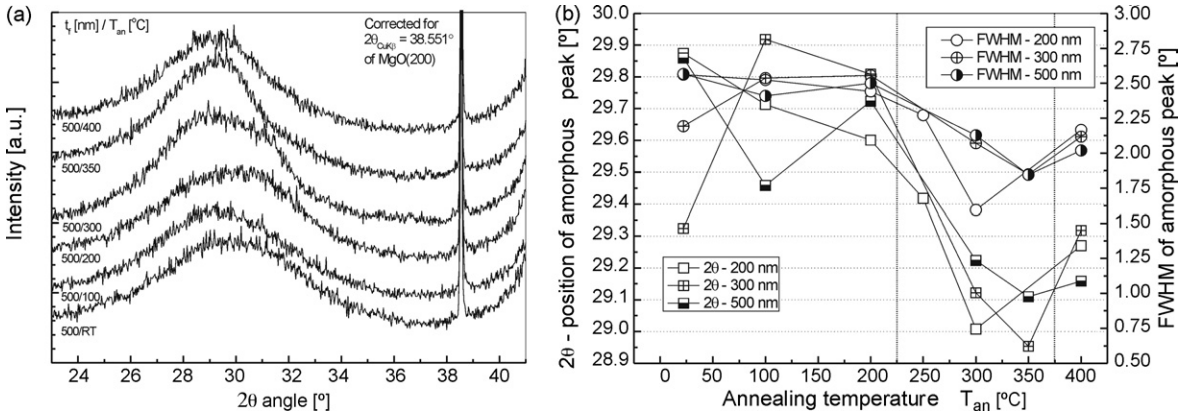

Fig. 1. (a) XRD patterns, and (b) 2θ-angle positions of amorphous peaks and their FWHM values of as-deposited and at various temperatures post-annealed PZT films with the thickness of 500 nm.

thicknesses of 200, 300, and 500 nm, and thus the corrected XRD data were fitted to Gaussian amplitude functions. The 2θ-angle positions of fitted amorphous peaks and their FWHM values are collected in Fig. 1(b). Graphs clearly show how 2θ-angles and FWHM values have minimum between annealing temperatures 250 and 350 °C. In average, amorphous peaks are shifted ~0.65° downwards and FWHM values decrease about ~0.5° when post-annealing temperature increases from RT to 350 °C. These changes actually implement that the interatomic distances and their distribution in the films have decreased, although there is no evidence of formation of any crystalline order and films are still amorphous. In the case of metal alloys, similar XRD peak behavior have been found, and it could be related to relaxation processes of macroscopic stress, due to peak shift, and microscopic stress, due to peak narrowing, respectively.[8] However, as it will be shown and discussed below, there are some other phenomena involved with these amorphous films that have to be considered. When post-annealing temperature was further increased to 400 °C, both 2θ-angle and FWHM values started to increase again. In the case of thinner films with the thickness of 200 and 300 nm, this increase could be related to initiation of the growth of low temperature intermediate phases, such as α-PbO and β-PbO that also affected the amorphous volume still present in the films. No pyrochlore phases could be observed in these films under the post-annealing temperature of 500 °C.[14]

Surface morphology of the films was characterized using SPM analysis. In Fig. 2(a), there is a SPM micrograph of the 200 nm thick film post-annealed at 250 °C shown, and in Fig. 2(b), surface roughness R_q values of PZT films with thicknesses of 200, 300, and 500 nm post-annealed at various temperatures are presented. From the SPM micrograph it can be concluded that the 200 nm film annealed at 250 °C is very flat with the surface roughness $R_q \approx 0.22$ nm. In Fig. 2(b), the R_q values of all the samples are collected together, and for the comparison, typical values of pure perovskite PZT films annealed at 700 °C were added. Also in Fig. 2(b), similar minimum of R_q values of PZT films with different thicknesses was found as it was found in the case of 2θ-angle and FWHM values in Fig. 1(b). Flattening of the sample surface takes place typically due to melting process or due to glass transformation process.[2] For the glass transformation temperature T_g, it is also characteristic to decrease with decreasing film thickness under some critical value due to enhanced presence of free surface in comparison to volume of the film.[7] Tendency is also seen in Fig. 2(b),

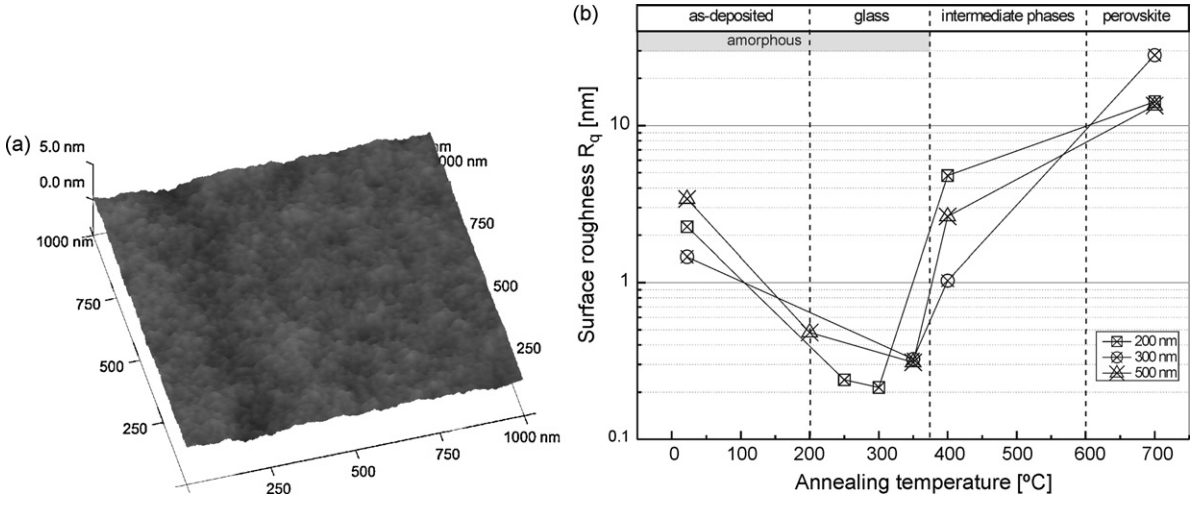

Fig. 2. (a) SPM micrograph of the 200 nm thick film post-annealed at 250 °C, and (b) surface roughness R_q values of PZT films with thicknesses of 200, 300, and 500 nm post-annealed at various temperatures. Approximate division of phase development as a function of temperature is also shown.

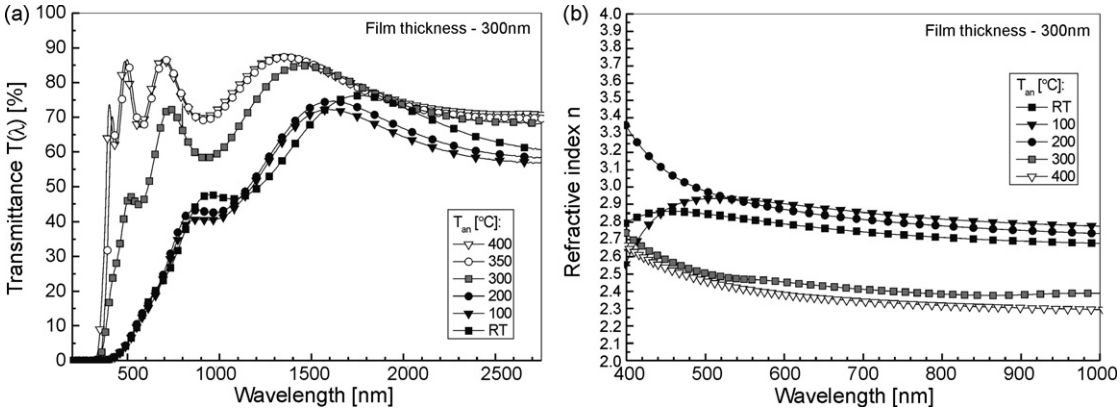

Fig. 3. (a) Transmittance $T(\lambda)$ spectra, and (b) calculated values of refractive index n at UV–vis–NIR wavelengths of as-deposited and at various temperatures post-annealed PZT films with the thickness of 300 nm.

although the number of different thicknesses is only three. By combining data from Figs. 1 and 2, it is possible to conclude that glass transformation takes place in amorphous PZT thin-films at the annealing temperature range $T_g \approx 250$–$350\,^{\circ}C$. Again, when post-annealing temperature was increased to 400 °C and above, the surface roughness started to increase due to growth of the crystalline structure and increasing size of the grains, and reached values $R_q \approx 10$–20 nm typical for ferroelectric PZT films with composition near MPB consisting of both trigonal and tetragonal grains.[14] Approximate division of phase development as a function of annealing temperature is also shown in Fig. 2(b).

Optical properties of some amorphous material groups, for example, silicate- and alumina-based oxide compounds, are changed remarkably when the glass transformation process takes place during the heat-treatment process.[2] Although materials are very transparent after forming glass, they are still found to be amorphous according to XRD measurements, and thus there has to be some phenomena other than just the previously mentioned stress relaxation causing the change in optical properties. These might include formation of chemical bonds between metal and oxygen ions without forming a periodic crystal structure, or growth of the nanocrystals of size below the smallest coherently diffracting domain detectable by XRD technique, for example. Such nanocrystals should also be transparent due to size at UV–vis–NIR wavelengths. Also, optical properties of PZT films studied here were changed remarkably when samples were annealed at temperatures from RT to 400 °C. In Fig. 3(a), there are shown six transmittance $T(\lambda)$ spectra measured at UV–vis–NIR wavelengths from 170 to 3000 nm of PZT films with the thickness of 300 nm. As-deposited PZT film and the films post-annealed at 100 and 200 °C have similar spectra with low transmittance $T(\lambda) < 25\%$ at UV–vis wavelengths. When the heat-treatment temperature was increased to glass transition temperature range $T_g \approx 250$–$350\,^{\circ}C$, transmittance of the films increased gradually close to, and even to higher values that are typically found in nanocrystalline perovskite PZT with $T(\lambda) > 86\%$ at interference maxima.[14,15] It is clearly seen from Fig. 3(a) that when 2θ-angle and FWHM values depicted in Fig. 1(a), and surface roughness R_q value in Fig. 2(b) are minimized, the transmittance reaches its maximum value at the same post-annealing temperature. In the case of 200 and 500 nm thick films, the transmittance behavior was essentially similar to that of 300 nm thick film, only with the exception of 200 nm film that actually reached its maximum transmittance already at the temperature of 300 °C. This result further supports the previously mentioned idea of thickness dependent glass transformation temperature T_g. From the optical and XRD data it is suggested that changes of $T(\lambda)$ properties are most likely due to formation of chemical bonding between metal (Ti^{4+}, Zr^{4+}, Pb^{2+}) and oxygen (O^{2-}) ions in glass transformation process, preferably Pb–O bonds, that act later as nucleation centers for the observed nanocrystalline α-PbO and β-PbO phases. Also the interference patterns of $T(\lambda)$ were behaving consistently in all samples, and the number of maxima was increasing and they were shifting towards shorter wavelengths when heat-treatment temperature increased. Because the films were of same thickness, this effect has to be due to change in optical length of the films $d_{opt} = n \times t_f$, where t_f stand for the film thickness. From this it can be concluded that films annealed below T_g have higher n and d_{opt} shifting the interference maximum of certain order to higher wavelengths. This is actually proved by the calculated data of refractive indices shown in Fig. 3(b). Values of n were calculated from $T(\lambda)$ graphs by fitting data to multiple Lorentz-oscillator model. Films annealed at temperatures below T_g had clearly higher refractive index values $n \approx 2.9$ at the wavelength of 600 nm, whereas the films processed at higher temperatures had values of around $n \approx 2.4$, which is pretty much of the same order that was measured from nanocrystalline perovskite PZT films.[15] This is actually in contradiction to the results reported by Xu et al. of the sol–gel derived amorphous PZT films,[5] but in quite good agreement with results reported by Hu et al. of rf magnetron sputtered films.[12] In the case of sol–gel derived amorphous films, the optical properties are most likely determined mainly by the organic residuals and pores left in the films after low temperature processing, and density of the films is quite low, whereas rf magnetron sputtering and PLD grown films are very dense even as as-deposited films due to the nature of deposition method.

By combining the results presented in Figs. 1–3 and discussion above, it is possible to conclude the total sequence of various phases formed during the crystallization process of

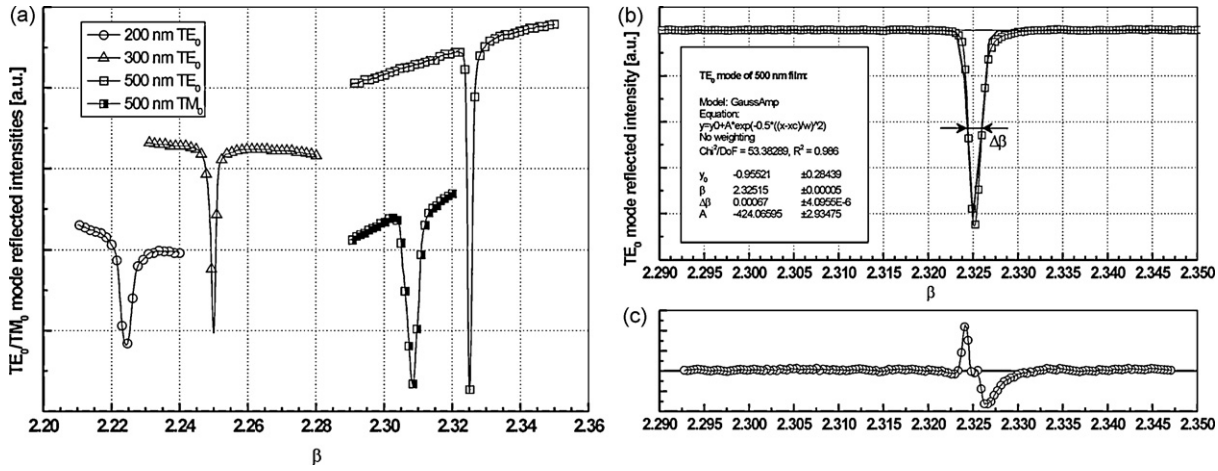

Fig. 4. (a) Optical TE_0 modes prism coupled to PZT films with the thickness of 200 and 300 nm, and TE_0 and TM_0 modes coupled to 500 nm thick film post-annealed at 400 °C. (b) Gaussian amplitude function fitting and (c) residual of the fit to TE_0 mode of 500 nm thick PZT film post-annealed at 400 °C.

PLD grown PZT thin-films. Previously, several groups have reported that amorphous PZT crystallizes through intermediate pyrochlore phases ($A_2B_2O_6$, etc.) to final perovskite ABO_3 phase.[16] Löbmann et al. have observed the formation of α-PbO low-temperature phase in post-annealed aerogels containing pure lead in the starting material.[17] In addition to these observations, it is now possible to add glass transformation process in the final heat-treatment procedure so that the final sequence will be: (i) as-deposited amorphous → (ii) glass → (iii) Pb-O, Ti-O, etc. → (iv) pyrochlore → (v) perovskite.

Optical waveguiding properties of the PZT films were also characterized using prism coupling method, in which a laser beam with wavelength of 632.8 nm is coupled into the films using a prism pressed against thin film surface, and photodiode is used to detect the reflected light from the film. When conditions for characteristic propagation constant β are fulfilled, the intensity of the laser light is actually coupled into the film, and the reflected light intensity from the prism decreases drastically. The FWHM value $\Delta\beta$, as described in Fig. 4, can be used as a light coupling quality factor for waveguiding materials. In Fig. 4(a), there are three different TE_0, and one TM_0 coupling modes of PZT films post-annealed at 400 °C shown. For the 200 nm thick film, that actually consisted also nanocrystalline α-PbO and β-PbO minor phases according to XRD measurements, the TE_0 mode was found to be relatively broad in comparison to others, and also, the drop in the reflected intensity was quite modest. However, in the case of 500 nm thick film, the coupled TE_0 mode was very narrow with FWHM values of $\Delta\beta \approx 0.00067$, as shown in Fig. 4(b) and (c), where Lorentz function fitting and the residual for measured optical mode data were calculated. Such values of $\Delta\beta$ are smaller than, for example, those for epitaxial $BaTiO_3$ films and very promising when the use of amorphous PZT thin-films in optical waveguiding applications are considered. Observed difference of β values between the TE_0 and TM_0 modes of 500 nm thick film indicates that there is also a birefringence effect in the films involved, probably due to residual macroscopic stresses generated during the deposition and thermal heat-treatment processes.

4. Conclusions

A new amorphous glassy phase of PLD deposited PNZT films with high optical transmittance $T(\lambda)$, refractive index n, and very good optical waveguiding properties $\Delta\beta \approx 0.00067$ was observed. Post-annealing heat treatment was started at 100 °C, and when temperature was increased above 250 °C, the optical transmittance of the films at all wavelengths increased remarkably and the morphology of the films was significantly improved down to the surface roughness values of $R_q \approx 0.2$ nm. Combining these changes with findings of XRD measurements, it was concluded that films went through glass transformation process with the characteristic temperature $T_g \approx 250$–350 °C. Due to excellent optical waveguiding properties and high refractive index $n > 2.4$, amorphous-like PZT thin-films are promising when optical waveguiding applications are considered.

Acknowledgements

Part of this work was carried out in the Micro- and Nanotechnology Center (MNT) of University of Oulu. J.P. acknowledges the financial support of Tauno Tönning Foundation.

References

1. Sze, S. M., *Physics of Semiconductor Devices*. John Wiley & Sons Inc., New York, 1981, p. 852.
2. Tangeman, J. A., Phillips, B. L. and Hart, R., Nucleation of perovskite nanocrystals in a levitating liquid. *J. Am. Ceram. Soc.*, 2007, **90**, 758–762.
3. Zhao, Z. F., Zhang, Z., Wen, P., Pan, M. X., Zhao, D. Q., Wang, W. H. and Wang, W. L., A highly glass-forming alloy with lowglass transition temperature. *Appl. Phys. Lett.*, 2003, **82**, 4699–4701.
4. Wei, J. and Gan, F., Theoretical explanation of different crystallization processes between as-deposited and melt-quenched amorphous $Ge_2Sb_2Te_5$ thin films. *Thin Solid Films*, 2003, **441**, 292–297.
5. Xu, Y., Cheng, C. H. and Mackenzie, J. D., Electrical characterizations of polycrystalline and amorphous thin films of $Pb(Zr_xTi_{1-x})O_3$ and $BaTiO_3$ prepared by sol–gel technique. *J. Non-Cryst. Solids*, 1994, **176**, 1–17.
6. Ray, C. S., Zhang, T., Reis, S. T. and Brow, R. K., Determining kinetic parameters for isothermal crystallization of glasses. *J. Am. Ceram. Soc.*, 2007, **90**, 769–773.

7. Forrest, J. A., Dalnoki-Veress, K., Stevens, J. R. and Dutcher, J. R., Effect of free surfaces on the glass transition temperature of thin polymer films. *Phys. Rev. Lett.*, 1996, **77**, 2002–2005.
8. Cullity, B. D., *Elements of X-ray Diffraction*. Addison-Wesley Publishing Company Inc., Reading, Massaschusetts, 1967, pp. 263–269.
9. Lines, M. E., Microscopic model for a ferroelectric glass. *Phys. Rev. B*, 1977, **15**, 388–395.
10. Glass, A. M., Lines, M. E., Nassau, K. and Shiever, J. W., Anomalous dielectric behaviour and reversible pyroelectricity in roller-quenched $LiNbO_3$ and $LiTaO_3$ glass. *Appl. Phys. Lett.*, 1977, **31**, 249–251.
11. Besher, E., Xu, Y. and Mackenzie, J. D., New low temperature multiphase ferroelectric films. *J. Appl. Phys.*, 2001, **89**, 6341–6348.
12. Hu, Z., Huang, Z., Lai, Z., Wang, G. and Chu, J., Optical properties of amorphous $Pb(Zr_xTi_{1-x})O_3$ ($x = 0.52$) thin films prepared by RF magnetron sputtering. *Thin Solid Films*, 2003, **437**, 223–229.
13. Lappalainen, J. and Lantto, V., Composition and phase structure in laser deposited and post-annealed $Pb_{1-3y/2}Nd_y(Zr_xTi_{1-x})O_3$ thin films. *Appl. Surf. Sci.*, 2000, **154–155**, 118–122.
14. Puustinen, J., Lappalainen, J., Hiltunen, J. and Lantto, V., Variations of optical properties with phase co-existence PZT thin films. *Ferroelectrics*, 2008, **370**, 46–56.
15. Lappalainen, J., Hiltunen, J. and Lantto, V., Characterization of optical properties of nanocrystalline doped PZT thin films. *J. Eur. Ceram. Soc.*, 2005, **25**, 2273–2276.
16. Kwok, C. K. and Desu, S. B., Pyrochlore to perovskite phase transformation in sol–gel derived lead–zirconate–titanate thin films. *Appl. Phys. Lett.*, 1992, **60**, 1430–1432.
17. Löbmann, P., Glaubitt, W., Geis, S. and Fricke, J., Monolithic crystalline lead zirconate titanate aerogels. *J. Non-Cryst. Solids*, 1998, **225**, 130–134.